ovarian cancer-specific EMT signatures were derived using a similar procedure (apart from Steps 1 and 2 depicted in Figure 1A) and were published elsewhere (Akalay *et al*, 2013; Miow *et al*, 2014); these were derived from comparing the profile of immunofluorescence staining of CDH1 and CDH2 (Materials and Methods). Since the cancer-specific EMT signatures were derived using the same procedure and have good correlation with the generic EMT signature (Table E1C), we performed additional analyses to verify only the validity of bladder cancer-specific EMT signature. The result is added in Fig. E1, Results section, and Expanded View of the revised manuscript.

Comment 2

Figure 3 and E2. It is claimed by the authors that EMT status does not necessarily correlate with poorer survival. Did the authors try performing the analyses after stratifying patients based on different subtypes of the same cancer? For example, will performing Kaplan-Meier analysis by subtypes of tumors (e.g. luminal, basal, ERBB2+, triple-negative subtypes of breast cancer) give a different result?

Response: We focused our analysis on correlating EMT status and survival only in molecular subtypes of breast cancer, as the molecular subtypes of breast cancer is more established (Prat *et al*, 2012). When stratified by molecular subtype, we observed a better disease-free survival (DFS) in patients with Basal and Claudin-Low breast cancers of a low EMT score than in those with a high EMT score (hazard ratio=0.6549, p=0.0089). There was no significant difference in other breast cancer subtypes when correlating EMT and DFS or overall survival. However, the correlation of EMT and DFS in Basal and Claudin-Low subtypes was not coherent in all breast cancer cohorts, probably due to the smaller sample sizes. Therefore, we did not report this finding initially. As pointed out by Referee#3, it might be of great interest to the reader, and we have added these results to Fig. E7, as well as the Results and Discussion sections.

Comment 3:

Figure 3 and E2. Given the critical roles of EMT in tumor cell dissemination and cancer metastasis, it is suggested that the authors also check metastasis-free survival, not only OS and DFS.

Response: We thank the Referee for pointing this out, as this made us aware that we were not clear in the definition of disease-free survival (DFS). The definition of DFS we adopted in the manuscript broadly encompassed (local) recurrence-free survival, progression-free survival, and distant metastasis-free survival (DMFS). The majority of the data were in fact distant metastasis-free survival. We have indicated in Fig. 3B which cohort data are DMFS, and inserted the definition of DFS in the text.

Comment 4:

There is growing evidence suggesting that the reversal of EMT, the mesenchymal-epithelial transition (MET), may be necessary for efficient metastatic colonization. The authors should discuss this point and the potential complications in the interpretation of their results.

Response: We thank the reviewer for raising this important point. Tsai et al. is a landmark paper and we fully agree with Tsai et al. as well as with Referees#2 and #3 that reversing EMT may promote metastatic colonization. This paradigm, to an extent, fits our previously proposed model where mesenchymal micro-metastases must re-acquire an epithelial phenotype to proliferate at the metastatic site (Thiery, 2002). The original text in the manuscript was not accurate ("the EMT reversion therapy as a means to reduce the metastatic potential") in that we are not postulating that EMT reversal therapy could *cure* metastasis, but instead we meant that EMT reversal therapy may *sensitize* cancer cells to specific drugs. Furthermore, our intent was not to achieve a full reversal of EMT—which, as pointed out by Referees#2, #3 and Tsai et al. could be detrimental—rather, we were referring to modifying the EMT status *along the spectrum* to improve patient responses to treatment. In our experience, the use of a single agent does not fully reverse EMT but it is sufficient to reduce invasion (unpublished), anoikis resistance, spheroidogenesis and clonogenicity *in vitro* (Huang *et al*, 2013), and *in vivo* using orthotopic grafting of a human cancer line (Sim & Thiery, 2014; manuscript in preparation). The main challenge, however, is that we do not know exactly at which intermediate states and under what conditions or context cancer cells in the primary—or at the distant sites—can exit dormancy and resume growth or develop chemo-resistance. This is a very complex problem requiring further investigations which are beyond the scope of the current study. We have amended the sentence to better reflect what we meant in the Discussion section of the revised manuscript.

Minor concerns:

1. What are the values of the y axis in Figure 1C (top panel)?

Response: We have put in the y-axis values on the top panel of Figure 1C.

References

Akalay I, Janji B, Hasmim M, Noman MZ, Andre F, De Cremoux P, Bertheau P, Badoual C, Vielh P, Larsen AK et al (2013) Epithelial-to-mesenchymal transition and autophagy induction in breast carcinoma promote escape from T-cell-mediated lysis. Cancer research 73: 2418-2427

Arumugam T, Ramachandran V, Fournier KF, Wang H, Marquis L, Abbruzzese JL, Gallick GE, Logsdon CD, McConkey DJ, Choi W (2009) Epithelial to mesenchymal transition contributes to drug resistance in pancreatic cancer. Cancer research 69: 5820-5828

Bauer JA, Chakravarthy AB, Rosenbluth JM, Mi D, Seeley EH, De Matos Granja-Ingram N, Olivares MG, Kelley MC, Mayer IA, Meszoely IM et al (2010) Identification of markers of taxane sensitivity using proteomic and genomic analyses of breast tumors from patients receiving

neoadjuvant paclitaxel and radiation. Clinical cancer research : an official journal of the American Association for Cancer Research 16: 681-690

Beasley GM, Riboh JC, Augustine CK, Zager JS, Hochwald SN, Grobmyer SR, Peterson B, Royal R, Ross MI, Tyler DS (2011) Prospective multicenter phase II trial of systemic ADH-1 in combination with melphalan via isolated limb infusion in patients with advanced extremity melanoma. Journal of clinical oncology : official journal of the American Society of Clinical Oncology 29: 1210-1215

The Cancer Genome Atlas Research (2012) Comprehensive molecular portraits of human breast tumours. Nature 490: 61-70

The Cancer Genome Atlas Research (2011) Integrated genomic analyses of ovarian carcinoma. Nature 474: 609-615

Carey LA, Rugo HS, Marcom PK, Mayer EL, Esteva FJ, Ma CX, Liu MC, Storniolo AM, Rimawi MF, Forero-Torres A et al (2012) TBCRC 001: randomized phase II study of cetuximab in combination with carboplatin in stage IV triple-negative breast cancer. Journal of clinical oncology : official journal of the American Society of Clinical Oncology 30: 2615-2623

Desmedt C, Giobbie-Hurder A, Neven P, Paridaens R, Christiaens MR, Smeets A, Lallemand F, Haibe-Kains B, Viale G, Gelber RD et al (2009) The Gene expression Grade Index: a potential predictor of relapse for endocrine-treated breast cancer patients in the BIG 1-98 trial. BMC medical genomics 2: 40

Donahue TR, Tran LM, Hill R, Li Y, Kovochich A, Calvopina JH, Patel SG, Wu N, Hindoyan A, Farrell JJ et al (2012) Integrative survival-based molecular profiling of human pancreatic cancer. Clinical cancer research : an official journal of the American Association for Cancer Research 18: 1352-1363

Erdem-Eraslan L, Gravendeel LA, de Rooi J, Eilers PH, Idbaih A, Spliet WG, den Dunnen WF, Teepen JL, Wesseling P, Sillevis Smitt PA et al (2013) Intrinsic molecular subtypes of glioma are prognostic and predict benefit from adjuvant procarbazine, lomustine, and vincristine chemotherapy in combination with other prognostic factors in anaplastic oligodendroglial brain tumors: a report from EORTC study 26951. Journal of clinical oncology : official journal of the American Society of Clinical Oncology 31: 328-336

Esserman LJ, Berry DA, Cheang MC, Yau C, Perou CM, Carey L, DeMichele A, Gray JW, Conway-Dorsey K, Lenburg ME et al (2012) Chemotherapy response and recurrence-free survival in neoadjuvant breast cancer depends on biomarker profiles: results from the I-SPY 1 TRIAL (CALGB 150007/150012; ACRIN 6657). Breast cancer research and treatment 132: 1049-1062

Evans AL, Faial T, Gilchrist MJ, Down T, Vallier L, Pedersen RA, Wardle FC, Smith JC (2012) Genomic targets of Brachyury (T) in differentiating mouse embryonic stem cells. PloS one 7: e33346

Farmer P, Bonnefoi H, Anderle P, Cameron D, Wirapati P, Becette V, Andre S, Piccart M, Campone M, Brain E et al (2009) A stroma-related gene signature predicts resistance to neoadjuvant chemotherapy in breast cancer. Nature medicine 15: 68-74

Frisch SM, Schaller M, Cieply B (2013) Mechanisms that link the oncogenic epithelial-mesenchymal transition to suppression of anoikis. Journal of cell science 126: 21-29

Gim J CY, Hong SH, Kim HC, Chun HK, Park T*, Park WY, Lee WY (2014) Predicting multi-class response to preoperative chemoradiotherapy in rectal cancer patients, manuscript in preparation.

Hao J, Zhang Y, Deng M, Ye R, Zhao S, Wang Y, Li J, Zhao Z (2014) MicroRNA control of epithelial-mesenchymal transition in cancer stem cells. International journal of cancer Journal international du cancer 135: 1019-1027

Hecker N, Stephan C, Mollenkopf HJ, Jung K, Preissner R, Meyer HA (2013) A new algorithm for integrated analysis of miRNA-mRNA interactions based on individual classification reveals insights into bladder cancer. PloS one 8: e64543

Hotz B, Arndt M, Dullat S, Bhargava S, Buhr HJ, Hotz HG (2007) Epithelial to mesenchymal transition: expression of the regulators snail, slug, and twist in pancreatic cancer. Clinical cancer research : an official journal of the American Association for Cancer Research 13: 4769-4776

Huang RY, Chung VY, Thiery JP (2012) Targeting pathways contributing to epithelial-mesenchymal transition (EMT) in epithelial ovarian cancer. Current drug targets 13: 1649-1653

Huang RY, Wong MK, Tan TZ, Kuay KT, Ng AHC, Chung VY, Chu Y-S, Matsumura N, Lai H-C, Lee YF et al (2013) An EMT Spectrum defines an anoikis resistant and spheroidogenic Intermediate Mesenchymal state that is sensitive to E-cadherin restoration by a Src-kinase inhibitor, Saracatinib (AZD0530). Cell Death and Disease: e915

Knudsen S, Jensen T, Hansen A, Mazin W, Lindemann J, Kuter I, Laing N, Anderson E (2014) Development and validation of a gene expression score that predicts response to fulvestrant in breast cancer patients. PloS one 9: e87415

Korde LA, Lusa L, McShane L, Lebowitz PF, Lukes L, Camphausen K, Parker JS, Swain SM, Hunter K, Zujewski JA (2010) Gene expression pathway analysis to predict response to neoadjuvant docetaxel and capecitabine for breast cancer. Breast cancer research and treatment 119: 685-699

Lehmann BD, Bauer JA, Chen X, Sanders ME, Chakravarthy AB, Shyr Y, Pietenpol JA (2011) Identification of human triple-negative breast cancer subtypes and preclinical models for selection of targeted therapies. The Journal of clinical investigation 121: 2750-2767

Lim E, Vaillant F, Wu D, Forrest NC, Pal B, Hart AH, Asselin-Labat ML, Gyorki DE, Ward T, Partanen A et al (2009) Aberrant luminal progenitors as the candidate target population for basal tumor development in BRCA1 mutation carriers. Nature medicine 15: 907-913

Lionetti M, Biasiolo M, Agnelli L, Todoerti K, Mosca L, Fabris S, Sales G, Deliliers GL, Bicciato S, Lombardi L et al (2009) Identification of microRNA expression patterns and definition of a microRNA/mRNA regulatory network in distinct molecular groups of multiple myeloma. Blood 114: e20-26

Liu S, Cong Y, Wang D, Sun Y, Deng L, Liu Y, Martin-Trevino R, Shang L, McDermott SP, Landis MD et al (2014) Breast Cancer Stem Cells Transition between Epithelial and Mesenchymal States Reflective of their Normal Counterparts. Stem cell reports 2: 78-91

Massarweh S, Tham YL, Huang J, Sexton K, Weiss H, Tsimelzon A, Beyer A, Rimawi M, Cai WY, Hilsenbeck S et al (2011) A phase II neoadjuvant trial of anastrozole, fulvestrant, and gefitinib in patients with newly diagnosed estrogen receptor positive breast cancer. Breast cancer research and treatment 129: 819-827

Medema JP (2013) Cancer stem cells: the challenges ahead. Nature cell biology 15: 338-344

Mestdagh P, Hartmann N, Baeriswyl L, Andreasen D, Bernard N, Chen C, Cheo D, D'Andrade P, DeMayo M, Dennis L et al (2014) Evaluation of quantitative miRNA expression platforms in the microRNA quality control (miRQC) study. Nature methods

Miow QH, Tan TZ, Ye J, Lau JA, Yokomizo T, Thiery J-P, Mori S (2014) Epithelial-Mesenchymal Status Renders Differential Responses to Cisplatin in Ovarian Cancer. Oncogene in press

Mulligan G, Mitsiades C, Bryant B, Zhan F, Chng WJ, Roels S, Koenig E, Fergus A, Huang Y, Richardson P et al (2007) Gene expression profiling and correlation with outcome in clinical trials of the proteasome inhibitor bortezomib. Blood 109: 3177-3188

Nakajima S, Doi R, Toyoda E, Tsuji S, Wada M, Koizumi M, Tulachan SS, Ito D, Kami K, Mori T et al (2004) N-cadherin expression and epithelial-mesenchymal transition in pancreatic carcinoma. Clinical cancer research : an official journal of the American Association for Cancer Research 10: 4125-4133

Prat A, Bianchini G, Thomas M, Belousov A, Cheang MC, Koehler A, Gomez P, Semiglazov V, Eiermann W, Tjulandin S et al (2014) Research-based PAM50 subtype predictor identifies higher responses and improved survival outcomes in HER2-positive breast cancer in the NOAH study. Clinical cancer research : an official journal of the American Association for Cancer Research 20: 511-521

Prat A, Ellis MJ, Perou CM (2012) Practical implications of gene-expression-based assays for breast oncologists. Nature reviews Clinical oncology 9: 48-57

Silver DP, Richardson AL, Eklund AC, Wang ZC, Szallasi Z, Li Q, Juul N, Leong CO, Calogrias D, Buraimoh A et al (2010) Efficacy of neoadjuvant Cisplatin in triple-negative breast cancer. Journal of clinical oncology : official journal of the American Society of Clinical Oncology 28: 1145-1153

Subramanian A, Tamayo P, Mootha VK, Mukherjee S, Ebert BL, Gillette MA, Paulovich A, Pomeroy SL, Golub TR, Lander ES et al (2005) Gene set enrichment analysis: a knowledge-based approach for interpreting genome-wide expression profiles. Proceedings of the National Academy of Sciences of the United States of America 102: 15545-15550

Tam WL, Weinberg RA (2013) The epigenetics of epithelial-mesenchymal plasticity in cancer. Nature medicine 19: 1438-1449

Taylor BS, Schultz N, Hieronymus H, Gopalan A, Xiao Y, Carver BS, Arora VK, Kaushik P, Cerami E, Reva B et al (2010) Integrative genomic profiling of human prostate cancer. Cancer cell 18: 11-22

Thiery JP (2002) Epithelial-mesenchymal transitions in tumour progression. Nature reviews Cancer 2: 442-454

Thiery JP, Acloque H, Huang RY, Nieto MA (2009) Epithelial-mesenchymal transitions in development and disease. Cell 139: 871-890

Tomkiewicz C, Hans S, Mucchielli MH, Agier N, Delacroix H, Marisa L, Brasnu D, Aggerbeck LP, Badoual C, Barouki R et al (2012) A head and neck cancer tumor response-specific gene signature for cisplatin, 5-fluorouracil induction chemotherapy fails with added taxanes. PloS one 7: e47170

Verhaak RG, Tamayo P, Yang JY, Hubbard D, Zhang H, Creighton CJ, Fereday S, Lawrence M, Carter SL, Mermel CH et al (2013) Prognostically relevant gene signatures of high-grade serous ovarian carcinoma. The Journal of clinical investigation 123: 517-525

Zhang J, Ma L (2012) MicroRNA control of epithelial-mesenchymal transition and metastasis. Cancer metastasis reviews 31: 653-662

2nd Editorial Decision 04 August 2014

Thank you for the submission of your revised manuscript to EMBO Molecular Medicine.

We have now received the enclosed reports from the Reviewers that were asked to re-assess it.

As you will see the Reviewers 2 and 3 are now globally supportive. Reviewer 1 was not available and I therefore asked Reviewer 2 to evaluate your response and action to his/her comments. Reviewer 2 considered your reply to Reviewer 1 satisfactory. However, concerning the availability of the easy-to-use algorithm to calculate the EMT signature, while your explanation is deemed

satisfactory, s/he would like you to make the availability of the Matlab script clear in the revised manuscript. I have checked the manuscript and feel that you have clearly stated this availability in the Materials and Methods section. Therefore no further action is required on your part regarding this issue.

I am thus pleased to inform you that we will be able to accept your manuscript.

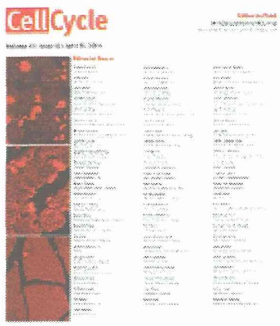

Cell Cycle
Publication details, including instructions for authors and subscription information:
http://www.tandfonline.com/loi/kccy20

Centrosomes at M phase act as a scaffold for the accumulation of intracellular ubiquitinated proteins

Hitomi Kimura[a], Yoshio Miki[ab] & Akira Nakanishi[a]

[a] Department of Molecular Genetics; Medical Research Institute; Tokyo Medical and Dental University (TMDU); Bunkyo-ku, Tokyo, Japan

[b] Department of Genetic Diagnosis; The Cancer Institute; Japanese Foundation for Cancer Research; Koto-ku, Tokyo, Japan

Published online: 17 Apr 2014.

REPORT

Cell Cycle 13:12, 1928–1937; June 15, 2014; © 2014 Landes Bioscience

Centrosomes at M phase act as a scaffold for the accumulation of intracellular ubiquitinated proteins

Hitomi Kimura[1], Yoshio Miki[1,2,*], and Akira Nakanishi[1]

[1]Department of Molecular Genetics; Medical Research Institute; Tokyo Medical and Dental University (TMDU); Bunkyo-ku, Tokyo, Japan; [2]Department of Genetic Diagnosis; The Cancer Institute; Japanese Foundation for Cancer Research; Koto-ku, Tokyo, Japan

Keywords: centrosome, ubiquitination, maturation, M phase, proteasome, proteome, cell cycle

Abbreviations: SILAC, stable isotope labeling by amino acids in cell culture; nano-LC–MS/MS, nano-liquid chromatography–tandem mass spectrometry; MS, mass spectrometry

Centrosome size varies considerably during the cell cycle; it is greatest during metaphase, partly because of pericentriolar matrix recruitment and an increase in microtubule-organizing activity. However, the mechanism of centrosome maturation during M phase is poorly defined. In the present study, we identified and quantified centrosomal proteins during S and M phases using stable isotope labeling by amino acids in cell culture (SILAC) coupled with liquid chromatography–tandem mass spectrometry (LC–MS/MS). We identified 991 proteins, of which 310 and 325 proteins were upregulated during S and M phases, respectively. Ubiquitinated proteins containing K48- and K63-linked polyubiquitin chains accumulated in the centrosomes during M phase, although 26S proteasome activity in the centrosomes did not markedly differ between S and M phases. Conversely, cytoplasmic dynein, which transports ubiquitinated proteins to the centrosomes, increased 2-fold in the centrosomes during M phase relative to S phase. Furthermore, PYR-41, a ubiquitin E1 inhibitor, reduced centrosome size during metaphase, causing increased aneuploidy. RNA interference suppression of Ecm29, which inhibits proteasome activity, decreased the accumulation of ubiquitinated proteins in the centrosomes. These results show that accumulation of ubiquitinated proteins promotes centrosome maturation during M phase and further suggest a novel function of centrosomes as a scaffold temporarily gathering intracellular ubiquitinated proteins.

Introduction

The centrosome is the main microtubule-organizing center. It comprises a pair of centrioles surrounded by amorphous pericentriolar material (PCM), and its size is tightly regulated during the cell cycle.[1] Centrosome maturation occurs at the onset of M phase and is accompanied by an increase in the size of PCM and its microtubule-nucleating capacity.[2] The centrosome is replicated between late G_1 and early S phases, whereupon it localizes to the spindle pole and participates in chromosome segregation during mitosis.[3,4]

Polo-like kinase 1 (Plk1) and Aurora A are reportedly involved in centrosome maturation.[5,6] Plk1 phosphorylates pericentrin (PCNT), and phosphorylated PCNT recruits centrosomal proteins, such as CEP192, GCP-WD, Aurora A, and γ-tubulin, into centrosomes.[2,7] CEP192 and nucleophosmin/B23 activates Aurora A, followed by phosphorylation of nudE neurodevelopment protein 1-like 1 (NDEL1) by Aurora A, thus leading to activation of centrosomal separation and centrosomal maturation.[8-10] In addition, ADP-ribosylated Miki and protein phosphatase 4 reportedly contribute to centrosome maturation.[11-13] Although the detailed mechanism underlying centrosome maturation remains unclear, its progression is important: inhibition of this process during mitosis causes chromosome missegregation and aneuploidy.[14,15]

Centrosomes contain an active 26S proteasome that degrades ubiquitinated proteins, and centrosomes become enlarged in response to proteasome activity inhibition and the resulting increase in misfolded proteins.[16-18] The 26S proteasome comprises 2 subcomplexes: the 20S catalytic core particle (CP) and the 19S regulatory particle (RP). Ecm29, a proteasome-associated protein, mainly associates with RP–CP complexes.[19] Ecm29 reportedly inhibits proteasome activity.[20,21]

Ubiquitinated proteins are transported to the centrosome by cytoplasmic dynein through HDAC6.[22] Ubiquitin is a 76-amino acid polypeptide, and 7 types of polyubiquitin chains have been identified in cells.[23] Ubiquitination with chains linked through lysine 48 leads to the degradation of substrate proteins at the 26S proteasome, whereas those linked via lysine 63 modulate protein–protein interactions during DNA repair,[24,25] signal

*Correspondence to: Yoshio Miki; Email: miki.mgen@mri.tmd.ac.jp
Submitted: 02/06/2014; Revised: 04/06/2014; Accepted: 04/14/2014; Published Online: 04/17/2014
http://dx.doi.org/10.4161/cc.28896

transduction,[26] and receptor endocytosis.[24] For example, K63-ubiquitinylated Tax, which maintains permanent NF-κB activation, localizes to the centrosome; however, little is known about the centrosome localization of K63-linked polyubiquitinated proteins.[27] The roles of polyubiquitin chains linked through K6, K11, K27, K29, or K33 are poorly understood.[23]

In this study, we investigated the mechanism of centrosome maturation. We showed that centrosome maturation during M phase is dependent on an increase in ubiquitinated proteins and occurs independently of proteasome activity. Furthermore, we verified that accumulated ubiquitinated proteins play an important role in centrosome function during mitosis.

Results

Centrosome maturation during M phase

We stained fixed HeLa S3 cells at specific stages of the cell cycle using an antibody specific for γ-tubulin. The centrosome cycle is synchronized to the cell cycle and consists of 4 phases, comprising centrosome duplication during S phase, centrosome maturation during the early mitotic phase, centrosome separation during metaphase, and centrosome disorientation during the late-mitotic G_1 phase (**Fig. 1A**). The intensity of centrosomal γ-tubulin immunofluorescence peaked at prometaphase and metaphase and then decreased significantly during anaphase (**Fig. 1A**; **Fig. S1A**). We measured centrosome size as indicated by γ-tubulin immunofluorescence staining during S phase and mitosis (**Fig. 1B**; **Fig. S1B**). The S phase centrosomes had a mean diameter of 0.57 ± 0.11 μm (n = 235). During mitosis, the diameter of each centrosome (1.32 ± 0.27 μm; n = 241) was approximately 2-fold greater than that during S phase ($P < 0.01$). We estimated the area of the centrosomes by quantifying the intensity of γ-tubulin immunofluorescence using Operetta™ (PerkinElmer Japan Co, Ltd; **Fig. S1C**). Compared with S phase, the size and intensity of the centrosomes significantly increased during M phase. PCM1, known to be necessary for the assembly of centrosome constituents such as centrioles was enriched around the centrosomes during G_1 and S phases; however, it had dispersed by prophase and largely disappeared by metaphase (**Fig. 1C**). This suggests that centrosome maturation during mitosis is independent of centrosome assembly by PCM1. Next, to investigate whether centrioles were more efficiently assembled in metaphase vs. S-phase centrosomes, we performed immunofluorescence microscopy on fixed HeLa S3 cells using an antibody against centrin1/2, a component of the centriole. We observed no significant change in the intensity of the centrin signal from G_1 phase to metaphase (**Fig. 1C**).

Components of the centrosome during S and M phases

We hypothesized that the centrosomal proteome differs between S and M phases. To test this hypothesis, we used the stable isotope labeling with amino acids in cell culture (SILAC) method (**Fig. 2A**). HeLa S3 cells were synchronized at M phase in "heavy" culture medium containing lysine labeled with a stable carbon-13 isotope (^{13}C-lysine) prior to centrosome isolation. In contrast, cells synchronized at S phase were cultured in "light" medium (containing ^{12}C-lysine) prior to centrosome isolation. We isolated centrosomes from HeLa S3 cells synchronized at S and M phases using a thymidine block, released them into mitosis 10 h later, and then determined the synchronicity of the cells using flow cytometry (**Fig. S2**). Two sets of centrosomes, prepared from a similar number of cells, were mixed and electrophoresed through 7.5% and 12.5% polyacrylamide gels stained with Coomassie brilliant blue (CBB) (**Fig. 2A**). The separated polypeptides were excised and identified using nano-liquid chromatography–tandem mass spectrometry (nano-LC–MS/MS). We identified 991 proteins, and the efficiency of peptide labeling was 97% (**Table S1**). We defined a protein as specifically present in the S- or M-phase centrosomes when the ionic strength ratio of the precursor ion of a peptide identified in both the heavy and light culture media was ≥1.5 and ≤0.67. A similar number of proteins was identified in the S-(310) and M-(325) phase centrosomes (**Fig. 2B**). This suggests that centrosome maturation during M phase is dependent upon cell cycle-dependent changes in the composition of the centrosomal proteome. The proteins identified in the 3 groups (S > M, S = M, and S < M) were classified according to their molecular functions using Gene Ontology (GO) database (**Fig. S3**). ATP-binding proteins were most frequently identified in all 3 groups. Although many RNA-binding proteins were identified in the groups S = M and S < M, it remains unclear why such proteins are present in the centrosome. Thirty-two centrosomal proteins identified by this proteomics analysis can be integrated with the cellular components (CC) documented in the Gene Ontology (GO) database. Other proteins, such as chaperones and RNA-binding proteins, are mostly congruent with those identified by analyses of other group.[28,29] Moreover, ubiquitinated proteins were 3-fold more abundant during M phase than during S phase (**Table S2**). However, the number of ubiquitinated proteins (37) was low relative to the number of proteins identified (991). To efficiently detect ubiquitinated proteins, they must be concentrated during the preparation of peptides for analysis by MS, and the original aim of this study was not to identify these ubiquitinated proteins.

Accumulation of ubiquitinated proteins in the centrosome during M phase

We hypothesized that centrosome maturation during M phase is dependent on the amount of ubiquitinated proteins. To test this hypothesis, we compared S- and M-phase centrosomes by immunoblot analysis using a multi-ubiquitin antibody (**Fig. 3A**, right panel). During M phase, the amount of ubiquitinated proteins in the centrosomes increased relative to that during S phase. Quantification of the signal showed an approximately 2-fold increase at M phase (**Fig. 3A**, lower panel). There was no difference in the amount of ubiquitinated proteins in whole-cell lysates (**Fig. 3A**, left panel). As a control, we confirmed that there was no difference in β-actin expression in whole-cell lysates and γ-tubulin in centrosome lysates (fractions 11 and 12) between M and S phases (**Fig. 3A**, left panel; **Fig. S4A**). Furthermore, we performed immunofluorescence microscopy of HeLa S3 cells using a multi-ubiquitin antibody (**Fig. 3B**, right panel). We observed an increase in the amount of ubiquitinated proteins in the

centrosomes during metaphase relative to that during interphase (Fig. 3B, 2 and 4 vs. 1 and 3). Furthermore, K63- (Fig. 3C, left panel) and K48- (Fig. 3C, right panel) linked protein–ubiquitin conjugates increased at M phase relative to S phase. There was no difference in the amount of γ-tubulin in centrosome lysates (fraction 11) between M and S phases (Fig. S4B).

Proteasome activity of the centrosome during S and M phases

Furthermore, we hypothesized that proteasome activity in centrosomes is higher during S phase than during M phase. To test this hypothesis, we added Z-LLE-AMC, a specific substrate of the proteasome, to the isolated centrosomes and measured the fluorescence intensity of its degradation products (Fig. 4A). A centrosome-enriched fraction (number 13) exhibited elevated proteasome activity. However, this activity decreased significantly when the proteasome inhibitor MG-132 was added to the assay system. Proteasome activity of the other fractions was similar to that of the centrosome-free preparation both in the presence and absence of MG-132. Unexpectedly, proteasome activity in the centrosomes was similar during M and S phases (Fig. 4B). There was a significant correlation between proteasome activity of the S- and M-phase centrosomes (Fig. 4C). This suggests that proteasome activity in centrosomes remains constant between phases and does not contribute to centrosome maturation.

Ubiquitinated proteins are reportedly transported by cytoplasmic dynein.[22,30] Levels of cytoplasmic dynein light chain 1 and dynein heavy chain 1, which are major components of cytoplasmic dynein, were found to be greater during M phase than

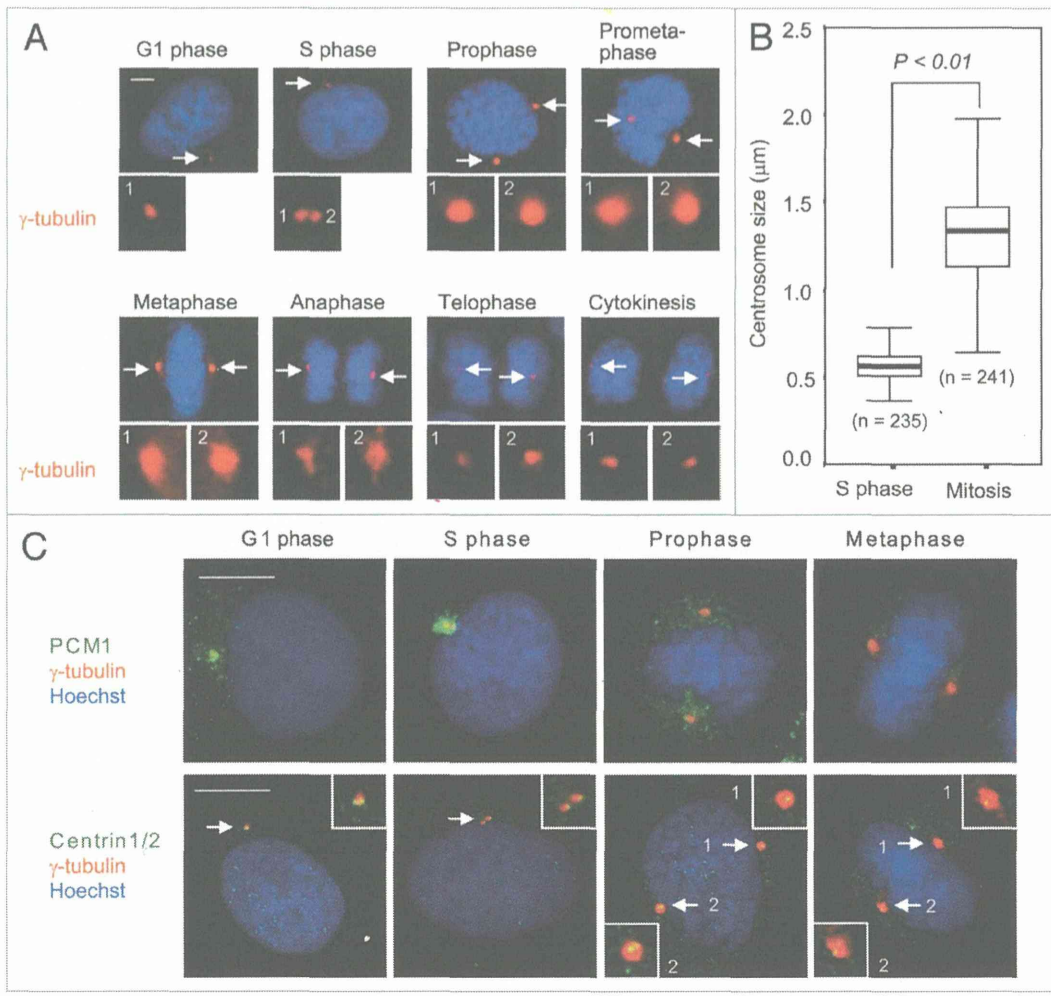

Figure 1. Centrosome size throughout the cell cycle. (**A**) Centrosomes in HeLa S3 cells were observed by immunofluorescence using the anti-γ-tubulin antibody as a marker (red, γ-tubulin). Inset: enlarged views. Arrow indicates location of centrosomes. Scale bars: 10 μm. (**B**) Estimation of centrosomal diameter following γ-tubulin immunofluorescence. The digital images were read using the ruler function in Photoshop CS5 (Adobe Systems Inc). The diameter of centrosomes at S (n = 235) and M (n = 241) phase is shown as a box plot that denotes the upper and lower quartiles. Boxes show the first and third quartiles, and whiskers mark minimum and maximum values unless they exceeded 1.5× the interquartile range. Statistical significance was determined using the Mann–Whitney *U* test ($P < 0.01$). Bold lines show medians. (**C**) Centrosomal pericentriolar material 1 (PCM1; top panel) and centrin1/2 (bottom panel) were visualized by immunofluorescence staining (red, γ-tubulin; green, PCM1 or centrin1/2). Arrow is localized at the centrosome and the inset shows enlarged views. DNA was stained with Hoechst (blue). Scale bars: 10 μm.

during S phase in centrosomes using SILAC-based proteomic analysis (**Table S1**). We measured dynein protein levels in the centrosomes during M and S phases by immunoblot analysis. The levels were 2.2-fold higher during M phase than during S phase (**Fig. 3A**, right panel). However, there was no difference in the levels of dynein in whole-cell lysates (**Fig. 3A**, left panel). Next, we investigated whether dynein depletion affects centrosome maturation. For this, we analyzed the effects of dynein knockdown using siRNA on the γ-tubulin staining of the centrosomes in metaphase cells (**Fig. S4C**). Compared with siRNA-treated control cells, centrosome size was diminished in dynein knockdown cells ($P < 0.01$). This demonstrates that centrosome maturation during M phase is dependent on dynein.

Ubiquitinated proteins are required for centrosome maturation

To prove that ubiquitinated proteins are involved in centrosome maturation during M phase, we evaluated HeLa S3 cells treated with the ubiquitin E1 inhibitor PYR-41 or DMSO (control) using antibodies against γ-tubulin and PCNA (an S phase marker; **Fig. 5A**). During metaphase, centrosome size decreased in PYR-41-treated cells compared with the control cells ($P < 0.01$; **Fig. 5B**). However, there was no significant difference in centrosome size during S phase. In addition, to confirm the importance of ubiquitinated centrosomal proteins during mitosis, we visualized chromosome segregation in PYR-41-treated HeLa S3 cells stably expressing green fluorescent protein (GFP)-HIST2H2B using time-lapse fluorescence microscopy (**Fig. 5C**). This revealed that 25% (22/86; **Fig. 5C**; type A) of metaphase cells progressed to anaphase with lagging chromosomes, and that 60% (51/86; **Fig. 5C**; type B) did not progress to anaphase, resulting in chromosome missegregation. The degradation of cyclin B1 is prerequisite for metaphase–anaphase transition. We demonstrated the decrease in cyclin B1 degradation at 30 min after the PYR41 treatment compared with the beginning (0 min) of the time-lapse observation by flow cytometry analysis using cyclin B1and phospho-Histone H3 (Ser10) antibodies (**Fig. S5**). This result suggests that the delay in the anaphase onset contribute to the attenuation of degradation of cyclin B1 by PYR-41 treatment. In contrast, the incidence of lagging chromosomes in the control cells was low (4% [4/93]; **Fig. 5C**; DMSO). Next, we examined microtubule nucleation during metaphase in HeLa S3 cells treated with PYR-41 or DMSO for 0, 5, 10, and 15 min. PYR-41 was washed out repeatedly to release the block, the cells were fixed,

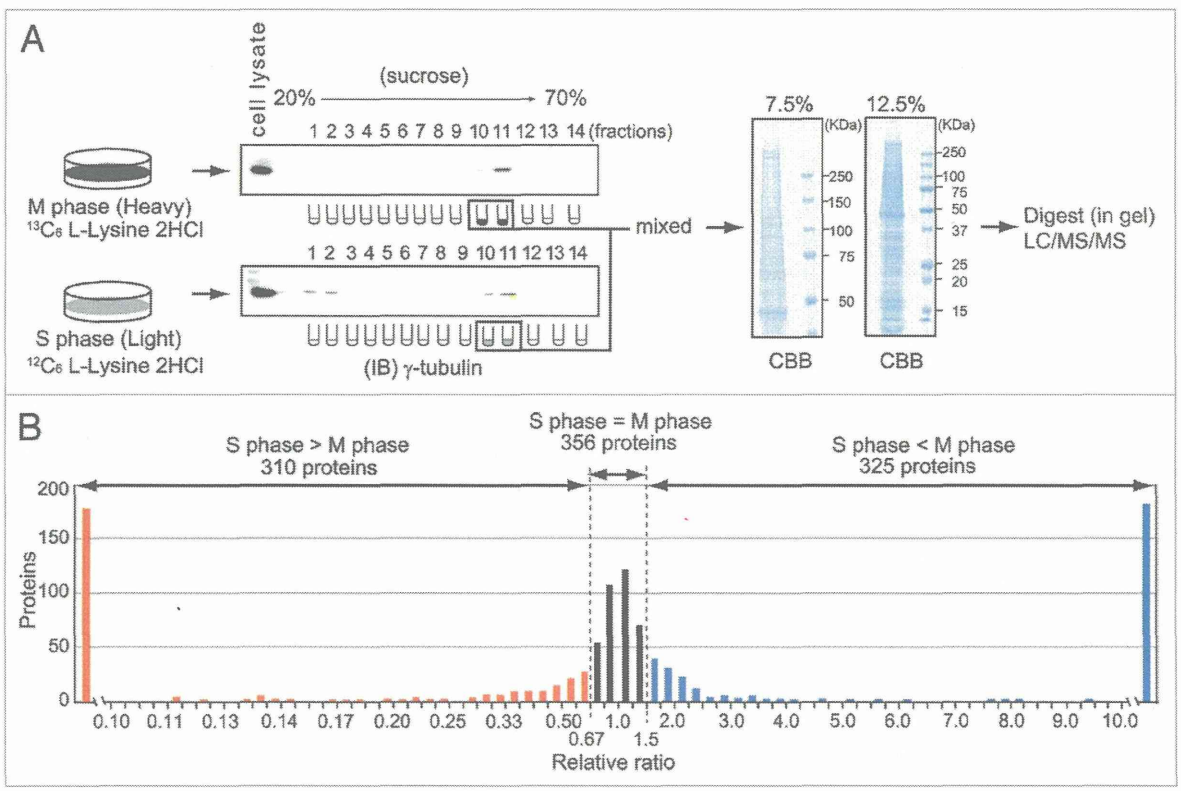

Figure 2. Analysis of centrosomal proteins in S and M phases by mass spectrometry. (**A**) Schematic outline of the stable isotope labeling by amino acids in cell culture (SILAC) method used to distinguish centrosomal proteins in S and M phases. Centrosomes were isolated from isotope-labeled and unlabeled cells by sucrose density gradient centrifugation. The centrosome-containing fractions were analyzed by immunoblotting using the anti-γ-tubulin antibody. The centrosome-containing fractions (10 and 11) were collected, fractionated by SDS–PAGE, mixed, digested, and analyzed by liquid chromatography–tandem mass spectrometry (LC–MS/MS). (**B**) The distribution of protein ratios. A total of 991 proteins were identified by SILAC: protein expression in S phase was 1.5-fold greater than that in M phase for 310 proteins (red bar); protein expression in M and S phase differed by less than 1.5-fold for 356 proteins (black bar); protein expression in M phase was 1.5-fold greater than that in S phase for 325 proteins (blue bar).

and metaphase cells were categorized according to the mitotic phase. The spindle fiber was assessed in metaphase cells by α-tubulin immunofluorescence (**Fig. 5D**, upper panel). In most PYR-41-treated cells, the spindle fiber was not evident (approximately 90% of cells over 15 min), and this effect was time-dependent (**Fig. 5D**, lower panel). Missegregation of chromosomes is known to cause aneuploidy; thus, we analyzed DNA index (DI) using flow cytometry to determine whether PYR-41-treated cells developed DNA aneuploidy (**Fig. 5E**). DI was represented by the ratio of the peak channel values of G_0/G_1 of HeLa S3 cells and PYR-41-treated HeLa S3 cells compared with that of normal human dermal fibroblasts (NHDFs, normal diploid cells). PYR-41-treated cells exhibited hyperdiploidy (DI = 1.57), whereas DI of control cells was 1.06. This suggests that inhibition of ubiquitin modification during M phase causes missegregation of chromosomes, leading to aneuploidy.

Ecm29 is associated with RP–CP complexes in the 26S proteasome and inhibits proteasome activity.[20,21] We isolated centrosomes from HeLa S3 cells treated with an siRNA against Ecm29 (**Fig. S6A**). Suppression of Ecm29 protein expression was confirmed by immunoblot analysis using an antibody against Ecm29 (**Fig. S6B**). Furthermore, we verified that the amount of ubiquitinated proteins in the centrosomes of Ecm29 siRNA-treated cells decreased compared with that in the centrosomes of control cells (**Fig. S6C**). As a control, we confirmed that the amount of β-actin was unaffected. We also isolated centrosomes from HeLa S3 cells treated with the proteasomal inhibitor MG-132 (**Fig. S6D**). Immunoblot analysis using a multi-ubiquitin antibody showed that the centrosomes of MG-132-treated cells contained an increased amount of ubiquitinated protein compared with those of control cells (DMSO-treated cells; **Fig. S6E**). We performed immunofluorescence microscopy on HeLa S3 cells treated with MG-132 or DMSO using an antibody against γ-tubulin. Compared with control cells, the centrosomes of MG-132-treated metaphase cells were enlarged (**Fig. S6F**). These results suggest that proteasome activity contributes to the amount of ubiquitinated proteins in the centrosome.

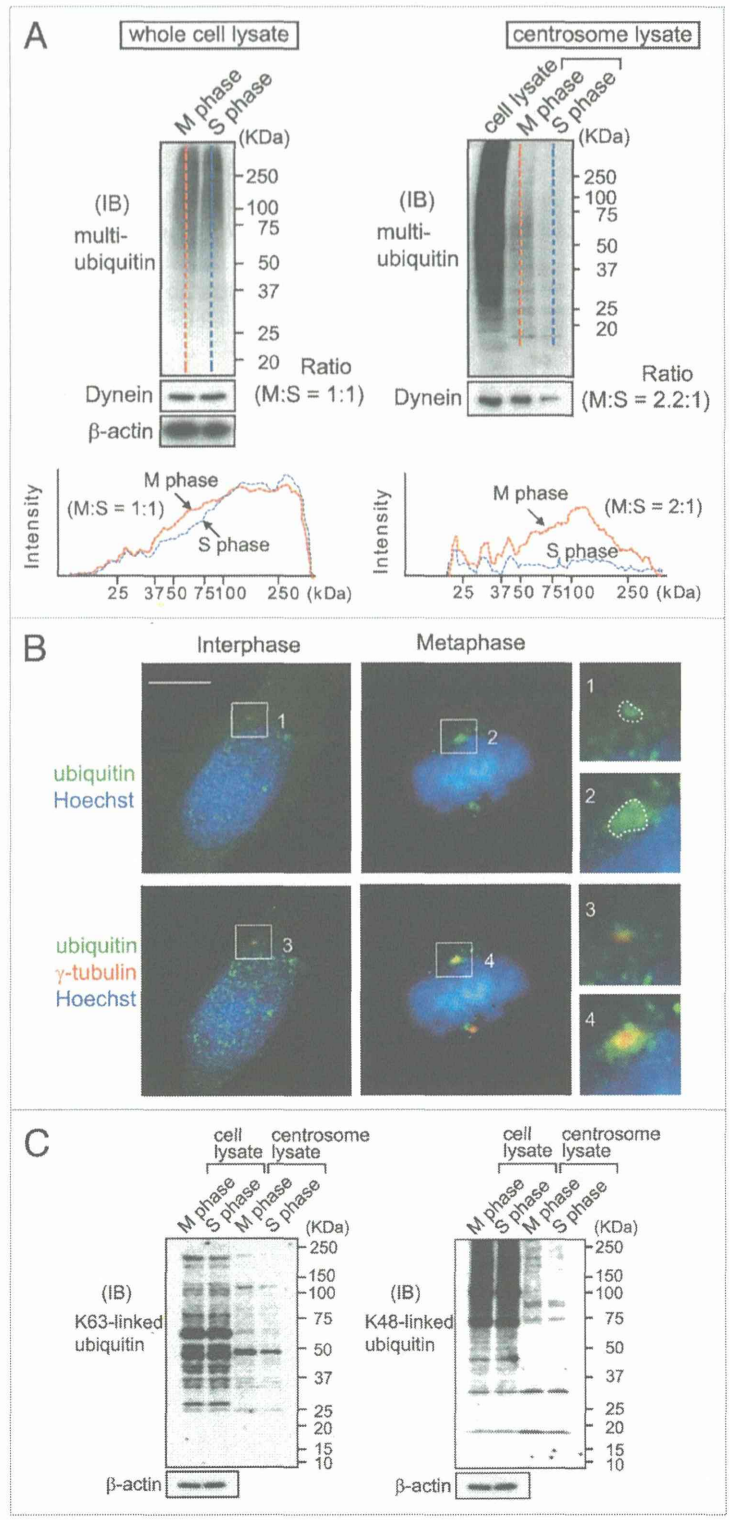

Figure 3. The augmentation of ubiquitinated proteins and cytoplasmic dynein at centrosomes in M phase. (**A**) Immunoblot analysis of ubiquitinated proteins and dynein in whole-cell (left panel) or centrosomal (right panel) lysates prepared from HeLa S3 cells synchronized at either S or M phase using antibodies against multi-ubiquitin or cytoplasmic dynein. Equivalent loading was determined by immunoblot analysis using an antibody against β-actin. Line scans measuring a broad band (15–300 kDa) of ubiquitin-associated relative fluorescence intensity are displayed, with the red and blue lines representing M phase- and S phase-specific ubiquitinated proteins, respectively. (**B**) HeLa S3 cells were fixed and subjected to co-immunofluorescence microscopy using ubiquitin (green) and γ-tubulin (red) antibodies. DNA was stained with Hoechst (blue). The boxed regions (the centrosome) are magnified. (**C**) Immunoblot analysis of ubiquitinated proteins in whole-cell or centrosomal lysates prepared from HeLa S3 cells synchronized at either S or M phase using antibodies against K63- (left panel) or K48- (right panel) linked polyubiquitin chains. Equivalent loading was determined by immunoblot analysis using an antibody against β-actin.

Discussion

We demonstrated that centrosome maturation proceeds by the accumulation of ubiquitinated proteins during M phase. This was deduced on the basis of the following 6 findings: (1) We identified and compared the relative abundance of proteins comprising the centrosome at M and S phases using the SILAC method and LC–MS/MS. Thirty-seven ubiquitinated proteins were identified, and many of these were detected in the centrosome during M phase (**Table S2**; M phase, 17 proteins; S phase, 5 proteins); (2) Immunoblot analysis using a multi-ubiquitin antibody revealed greater amounts of ubiquitinated proteins in the centrosome during M phase than during S phase (**Fig. 3A**, right panel); (3) Proteasome activity in the centrosome was similar during M and S phases (**Fig. 4B and C**); (4) The level of cytoplasmic dynein in the centrosome was greater during M phase than during S phase (**Fig. 3A**; **Fig. S4C**; **Table S1**); (5) The size of the centrosome during M phase was markedly decreased by inhibition of ubiquitination using PYR-41 (**Fig. 5A and B**); (6) Suppression of Ecm29, which inhibits proteasome activity, decreased the accumulation of ubiquitinated proteins in the centrosomes (**Fig. S6C**). Despite the similar amounts of ubiquitinated proteins in whole-cell lysates at M and S phases, increased amounts of ubiquitinated proteins were evident in the centrosome during M phase (**Fig. 3A**). These results suggest that the increase in the amount of ubiquitinated proteins in the centrosome is derived from the transport by cytoplasmic dynein, because there was no difference in proteasome activity between M and S phases.

Inhibition of ubiquitination prevents centrosome maturation and leads to abnormal spindle fiber formation, defective chromosome segregation, and chromosome aneuploidy (**Fig. 5C–E**). This suggests that ubiquitinated proteins participate in both maturation of the central body and chromosome separation. We identified 37 ubiquitinated proteins using SILAC and LC–MS/MS (**Table S2**). Of them, only Hsp90 reportedly localizes to the centrosomes. However, exactly which of its isoforms (Hsp90α or Hsp90β) localizes to the centrosome remains unclear. Using immunofluorescence microscopy with specific antibodies, we confirmed that Hsp90α, but not Hsp90β, localizes to the centrosome (data not shown). Furthermore, in most HeLa S3 cells subjected to siRNA-mediated knockdown of Hsp90α, the spindle fiber was not evident (data not shown). Hsp90 is a chaperone protein that combines with client proteins and participates in cell cycle progression, DNA repair,[31,32] and chromosome separation in response to heat shock or oxidative stress.[33] One such client protein is Plk1 that regulates centrosome function

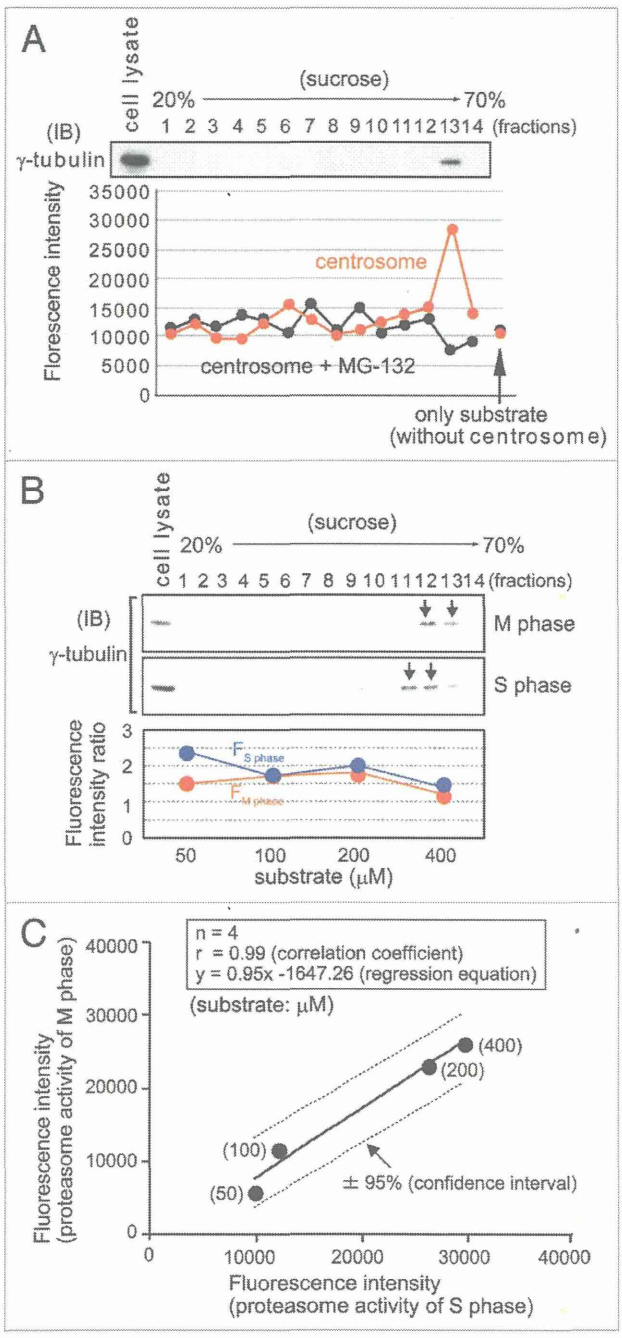

Figure 4. Proteasome activity of the centrosome between M and S phases. (**A**) Centrosomes were isolated by sucrose density gradient centrifugation. The centrosome-enriched fraction (13) was analyzed by immunoblotting using a γ-tubulin antibody. Proteolysis of the proteasome-specific fluorogenic substrate Z-LLE-AMC (fractions 1–14) was performed in the absence (red circles) or presence (black circles) of MG-132. The arrows show florescence intensity in each reaction without centrosomes. (**B**) Lysates from synchronized HeLa S3 cells at M or S phase fractionated by sucrose density gradient centrifugation and probed with a γ-tubulin antibody. The arrows indicate centrosome-enriched fractions used for proteasome activity (upper). Proteolysis of the proteasome-specific fluorogenic substrate Z-LLE-AMC, which was added to S- or M-phase centrosomes, and then analyzed by fluorescence spectroscopy of the liberated AMC on a microtiter plate reader (down). $F_{S\ phase}$ was calculated from the fluorescence intensity of proteasome activity of S-phase centrosomes against that without the centrosome (blue circle). $F_{M\ phase}$ was calculated from the fluorescence intensity of proteasome activity of M-phase centrosomes against that without the centrosome (red circle). (**C**) Pearson's correlation coefficients were used to show the relationships between the proteasome activity of S-phase and that of M-phase centrosomes. Each spot (black circle) shows the fluorescence intensity of S- and M-phase centrosomes with substrate (50, 100, 200, and 400 μM).

in a complex with Hsp90.[34] Inhibition of Hsp90 inactivates Plk1 activity and prevents microtubule nucleation.[35,36] Hsp90 is reportedly modified by K48-, K63-, K6-, and K11-linked ubiquitin chains.[37] We showed that K63-linked ubiquitinated proteins are present in the centrosome (Fig. 3C). Furthermore, we determined that K632 of Hsp90α is modified by ubiquitin in HeLa S3 cells (data not shown). These results suggest that K63-linked Hsp90–ubiquitin conjugates participate in centrosome maturation. In future studies, we hope to confirm whether K63-linked Hsp90–ubiquitin conjugates are present in the centrosome and cooperate with Plk1 to regulate centrosome maturation.

Inhibition of proteasome activity leads to the formation of the aggresome, believed to be an important structure for processing abnormal proteins in the cell. Cytoplasmic protein aggregates are transported to the centrosome.[38] In this study, we showed that many ubiquitinated proteins are transported to the centrosome during M phase, and that centrosomal proteasome activity remains constant during S and M phases. These findings suggest that the centrosome may act as a scaffold temporarily, not only functionally important ubiquitinated proteins but also integrating misfolded or damaged proteins produced during G_1 and M phases.

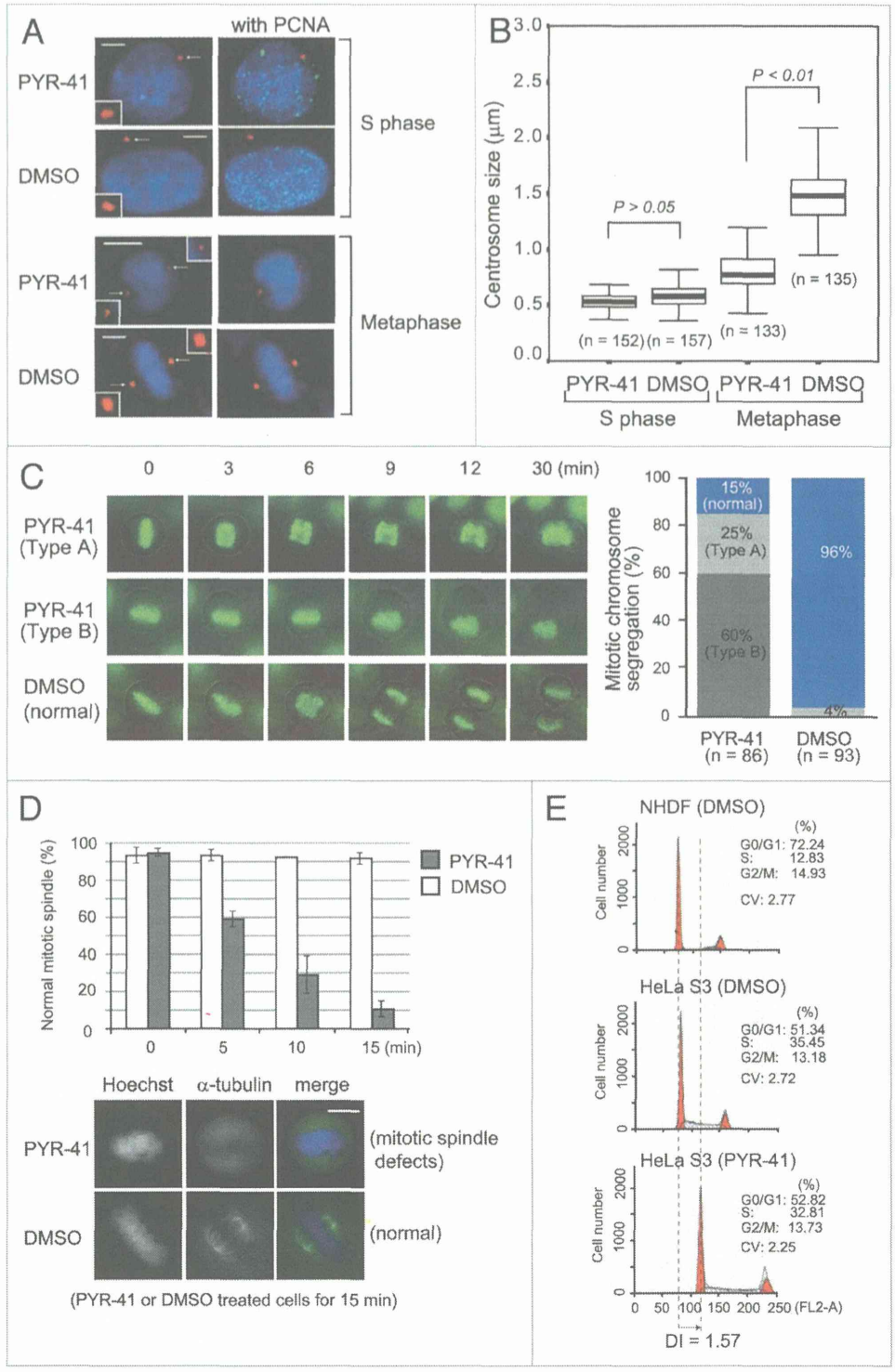

Figure 5. For figure legend, see page 1935.

Materials and Methods

Antibodies and siRNA

The following antibodies were used in this study: anti-Ecm29 (mouse, Sigma-Aldrich; rabbit, GeneTex); anti-β-actin (mouse, AC-74, Sigma-Aldrich); anti-γ-tubulin (mouse, Santa Cruz Biotechnology; rabbit, C-11, Sigma-Aldrich); anti-α-tubulin (rabbit, Abcam); anti-centrin1/2 (rabbit, H-40, Santa Cruz Biotechnology); anti-PCM1 (rabbit, G2000, Cell Signaling Technology); anti-dynein HC1 (rabbit, Santa Cruz

Figure 5 (See previous page). Centrosome maturation is associated with the presence of ubiquitinated proteins. (**A**) HeLa S3 cells treated with PYR-41 (a ubiquitin E1 inhibitor) or DMSO (control) for 1 d were subjected to immunofluorescence with antibodies against γ-tubulin (red) or PCNA (green). PCNA is an S-phase marker. Inset: higher magnification images of the region indicated by the arrows. (**B**) Size of centrosomes in cells treated with 50 g/ml PYR-41 or DMSO (control). Median centrosome diameter in cells in S (PYR-41: n = 152; DMSO: n = 157) or M (PYR-41: n = 133; DMSO: n = 135) phase is presented in a box plot denoting the upper and lower quartiles. Boxes show the first and third quartiles, and whiskers mark minimum and maximum values unless these exceed 1.5 the interquartile range. Statistical significance was determined using the Mann–Whitney *U* test. (**C**) Time-lapse series of HeLa S3 cells stably expressing a green fluorescent protein (GFP) fusion with histone H2B (left). The cells were treated with 50 g/ml PYR-41 (n = 86) or DMSO (n = 93) and imaged immediately. Time is shown in minutes. Quantification of chromosome segregation in HeLa S3 cells treated as described above and scores for normal segregation or abnormal morphologies (right). (**D**) Immunofluorescence microscopy of HeLa S3 cells treated with 50 g/ml PYR-41 or DMSO (control) for 0, 5, 10, and 15 min using an antibody against α-tubulin (green; bottom panel). Quantification of spindle phenotypes in HeLa S3 cells treated as described above and scored for normal morphology (upper panel). Data represent the average of 3 independent experiments s.e.m., each including at least 40 mitotic cells. DNA was stained with Hoechst (blue). Scale bars: 5 m. (**E**) DNA histograms by flow cytometry of normal diploid primary normal human dermal fibroblasts (NHDFs) (DNA index [DI] = 1.00), and HeLa S3 cells treated with PYR-41 (DI = 1.57) or DMSO (DI = 1.06).

Biotechnology); anti-ubiquitin (mouse, FK2, MBL, 6C1, Sigma-Aldrich; rabbit, serum, Thermo Scientific); anti-K48-linkage specific polyubiquitin (rabbit, Cell Signaling Technology); anti-K63-linkage specific polyubiquitin (rabbit, Cell Signaling Technology); and anti-PCNA (rabbit, Abcam). The siRNA oligonucleotides used for human Ecm29, cytoplasmic dynein 1 heavy chain 1 (dynein), and a nonspecific negative control were purchased from Dharmacon.

Cell culture, synchronization, and transfection

HeLa S3 cells derived from cervical cancer were cultured in Dulbecco modified Eagle medium (DMEM; Nissui Pharmaceutical) supplemented with 100 mM L-glutamine and 10% fetal bovine serum (GIBCO) in 10% CO_2 at 37 °C. Primary NHDFs (DS Pharma Biomedical) were cultured in CSC complete recombinant medium (DS Pharma Biomedical) containing cell boost (DS Pharma Biomedical) in 10% CO_2 at 37 °C.

HeLa S3 cells were synchronized at S phase using a double thymidine block. The cells were incubated for 18 h in 2.5 mM thymidine, washed in PBS, released for 9 h, and then blocked for another 15 h in 2.5 mM thymidine. M-phase cells were synchronized at S phase using a thymidine block and then released for 10 h. Both phases were examined using flow cytometry.

The cells were transfected with siRNAs using Lipofectamine RNAiMAX reagent (Invitrogen) at approximately 40% confluence in Opti-MEM 1 (Invitrogen) according to the manufacturer's instructions. MG-132 and PYR-41 were purchased from Merck. Thymidine was purchased from Wako.

Plasmid constructs and generation of stably expressing cells

HeLa S3 cells stably expressing GFP-HIST2H2B or GFP-α-tubulin were generated as follows. HIST2H2B was amplified by PCR using the forward primer 5′-TGTCTCGAGC CATGCCTGAA CCGGCAAAAT-3′ and the reverse primer 5′-GGCGAATTCT CACTTGGAGC TGGTGTAC-3′ and then inserted into pEGFP-C1 (pEGFP-C1-HIST2H2B vector; Clontech). All plasmids were verified by DNA sequencing.

HeLa S3 cells were transfected with the pEGFP-C1-HIST2H2B or pAcGFP1-tubulin plasmid vector (Clontech) using Lipofectamine LTX with Plus reagent (Life Technologies). GFP-expressing clones were initially isolated by G418 resistance selection (4 mg/ml). The selected clones were isolated by limited dilution cloning. All clones appeared to be stable and continued to express GFP-HIST2H2B or GFP-α-tubulin after >10 passages in the absence of G418.

DNA aneuploidy analysis by flow cytometry

The cells were harvested using trypsin, fixed in 70% ethanol, washed twice in PBS, resuspended in PBS containing 0.2% Triton X-100, and incubated with 100 μg/ml RNase A. The cells were then incubated with 10 μg/ml propidium iodide (Sigma-Aldrich). The DNA content of the cells was analyzed using FACSCalibur HG (BD Biosciences) and CellQuest Pro software.

Immunoblot analysis

HeLa S3 cells were harvested and washed twice in PBS. The cell pellet was suspended in lysis buffer (150 mM NaCl, 1% Nonidet P-40, 0.5% deoxycholate, 2% SDS, 50 mM Tris–HCl, and protease inhibitor). The cells were lysed on ice for 20 min and then centrifuged at 20400 × g for 30 min at 4 °C. The retrieved proteins were resolved by SDS-PAGE and transferred onto a PVDF membrane (Millipore). This membrane was incubated with a primary antibody for 1 h and then with a secondary antibody coupled to horseradish peroxidase (Amersham Biosciences) for 1 h. The blots were developed using the enhanced chemiluminescent reagent SuperSignal (Thermo Scientific Pierce).

Immunofluorescence

The cells were washed in PBS and fixed with 3.4% formaldehyde in PBS for 10 min. They were permeabilized using 50%, 75%, and 95% ethanol on ice for 5 min each, blocked in donkey serum for 30 min at room temperature, and then incubated with a primary antibody for 1 h. The cells were then incubated with Alexa-488- and Alexa-594-conjugated secondary antibodies for 30 min at 37 °C. DNA was stained with 1 μg/ml Hoechst 33258. The samples were observed using an Olympus Power BX51 fluorescence microscope (Olympus).

Centrosome isolation

Purified centrosomes were isolated from HeLa S3 cells according to the method described by Moudjou and Bornens.[39] The cells were harvested by centrifugation at 280 × g, washed once with a buffer containing 10 mM Tris–HCl (pH 7.4) and 150 mM NaCl, and once with the same buffer containing 8% (w/v) sucrose. The cells were lysed in the lysis buffer (1 mM HEPES [pH 7.2], 0.5% Nonidet P-40, 0.5 mM $MgCl_2$, 0.1% 2-mercaptoethanol, and protease inhibitor) until chromatin aggregates were visible and then centrifuged at 2500 × g for 10 min to remove nuclei and chromatin aggregates. The supernatant was adjusted to 10 mM HEPES and digested with 2 units/ml DNase I for 30 min on ice. The lysate was then overlaid onto 60% sucrose solution (60% w/w sucrose prepared in 10 mM PIPES [pH 7.2], 0.1% Triton X-100, and 0.1% 2-mercaptoethanol) and centrifuged at

10000 × g for 30 min. Centrosomes sedimented onto the cushion were resuspended and loaded onto a discontinuous gradient consisting of 70% sucrose at the bottom, followed by 50% and 40% layers, and centrifuged at 40000 × g for 1 h. Fractions were collected starting from the top of the gradient and diluted in 1 ml of 10 mM PIPES buffer (pH 7.2). The centrosomes were obtained by centrifugation at 16000 × g for 10 min. The centrosome-enriched fraction was identified by immunoblot analysis using anti-γ-tubulin, a centrosome marker.

Relative quantitative analysis by MS

HeLa S3 cells were grown asynchronously in custom-synthesized DMEM with normal L-lysine or isotope-labeled $^{13}C_6$ L-lysine (Thermo Scientific Pierce) in 5% CO_2 at 37 °C. The medium was supplemented with 10% dialyzed fetal bovine serum. The cells were cultured for at least 5 doublings to fully incorporate the SILAC amino acids and then synchronized at S phase (normal L-lysine) and M phase (isotope-labeled $^{13}C_6$ L-lysine). Centrosome-containing fractions from unlabeled cells (S phase) were added to fractions containing centrosomes from SILAC-labeled cells (M phase). Centrosomes from the resulting samples were pelleted by centrifugation at 16000 × g for 10 min. The centrosomal proteins were separated by SDS-PAGE (7.5% and 12.5% polyacrylamide gels) and in-gel-digested with trypsin. The resulting peptides were extracted and desalted. These were analyzed by QTRAP 5500 LC–MS/MS (AB SCIEX). All data were analyzed using ProteinPilot™ (AB SCIEX) to identify and quantify proteins. Proteins were classified according to their biological functions using gene ontology.

Chromosome segregation in PYR-41-treated HeLa S3 cells

HeLa S3 cells stably expressing pEGFP-C1-HIST2H2B in glass-bottomed dishes (Matsunami) were treated with 50 μg/ml PYR-41 and subjected to time-lapse immunofluorescence microscopy every 3 min for 30 min.

Proteasome activity assay

Isolated centrosomes were incubated with 200 μM Z-LLE-AMC (Boston Biochem) in reaction buffer (250 mM HEPES, 5 mM ATP, 50 mM $MgCl_2$, 500 mM NaCl, and 5 mg/ml BSA) at 37 °C for 30 min. Proteasome activity was analyzed by fluorescence spectroscopy of the liberated AMC at 380/440 nm excitation/emission on a microtiter plate reader (PerkinElmer). Centrosomes treated with 50 μM MG-132, a specific proteasome inhibitor, were also subjected to the same analysis.

Statistical analysis

Statistical significance was evaluated using a 2-tailed Mann–Whitney *U* test. Pearson correlation coefficients were used for pairwise correlations between variables (proteasome activity of S phase and M phase centrosomes).

Disclosure of Potential Conflicts of Interest

No potential conflicts of interest were disclosed.

Acknowledgments

We thank all members of the Miki lab for helpful discussions. We thank Dr Hiroko Saito for technical help. We are grateful to Masashi Isogai (PerkinElmer Japan Co, Ltd) for analysis of centrosome size by Operetta™. The authors would like to thank Enago (http://www.enago.jp) for the English language review.

Supplemental Materials

Supplemental materials may be found here:
www.landesbioscience.com/journals/cc/article/28896

References

1. Blagden SP, Glover DM. Polar expeditions--provisioning the centrosome for mitosis. Nat Cell Biol 2003; 5:505-11; PMID:12776127; http://dx.doi.org/10.1038/ncb0603-505
2. Lee K, Rhee K. PLK1 phosphorylation of pericentrin initiates centrosome maturation at the onset of mitosis. J Cell Biol 2011; 195:1093-101; PMID:22184200; http://dx.doi.org/10.1083/jcb.201106093
3. Hanashiro K, Brancaccio M, Fukasawa K. Activated ROCK II by-passes the requirement of the CDK2 activity for centrosome duplication and amplification. Oncogene 2011; 30:2188-97; PMID:21242972; http://dx.doi.org/10.1038/onc.2010.607
4. Mardin BR, Isokane M, Cosenza MR, Krämer A, Ellenberg J, Fry AM, Schiebel E. EGF-induced centrosome separation promotes mitotic progression and cell survival. Dev Cell 2013; 25:229-40; PMID:23643362; http://dx.doi.org/10.1016/j.devcel.2013.03.012
5. Bruinsma W, Raaijmakers JA, Medema RH. Switching Polo-like kinase-1 on and off in time and space. Trends Biochem Sci 2012; 37:534-42; PMID:23141205; http://dx.doi.org/10.1016/j.tibs.2012.09.005
6. Nikonova AS, Astsaturov I, Serebriiskii IG, Dunbrack RL Jr., Golemis EA. Aurora A kinase (AURKA) in normal and pathological cell division. Cell Mol Life Sci 2013; 70:661-87; PMID:22864622; http://dx.doi.org/10.1007/s00018-012-1073-7
7. Casenghi M, Meraldi P, Weinhart U, Duncan PI, Körner R, Nigg EA. Polo-like kinase 1 regulates Nlp, a centrosome protein involved in microtubule nucleation. Dev Cell 2003; 5:113-25; PMID:12852856; http://dx.doi.org/10.1016/S1534-5807(03)00193-X
8. Reboutier D, Troadec MB, Cremet JY, Fukasawa K, Prigent C. Nucleophosmin/B23 activates Aurora A at the centrosome through phosphorylation of serine 89. J Cell Biol 2012; 197:19-26; PMID:22451695; http://dx.doi.org/10.1083/jcb.201107134
9. Joukov V, De Nicolo A, Rodriguez A, Walter JC, Livingston DM. Centrosomal protein of 192 kDa (Cep192) promotes centrosome-driven spindle assembly by engaging in organelle-specific Aurora A activation. Proc Natl Acad Sci U S A 2010; 107:21022-7; PMID:21097701; http://dx.doi.org/10.1073/pnas.1014664107
10. Mori D, Yano Y, Toyo-oka K, Yoshida N, Yamada M, Muramatsu M, Zhang D, Saya H, Toyoshima YY, Kinoshita K, et al. NDEL1 phosphorylation by Aurora-A kinase is essential for centrosomal maturation, separation, and TACC3 recruitment. Mol Cell Biol 2007; 27:352-67; PMID:17060449; http://dx.doi.org/10.1128/MCB.00878-06
11. Ozaki Y, Matsui H, Asou H, Nagamachi A, Aki D, Honda H, Yasunaga S, Takihara Y, Yamamoto T, Izumi S, et al. Poly-ADP ribosylation of Miki by tankyrase-1 promotes centrosome maturation. Mol Cell 2012; 47:694-706; PMID:22864114; http://dx.doi.org/10.1016/j.molcel.2012.06.033
12. Martin-Granados C, Philp A, Oxenham SK, Prescott AR, Cohen PT. Depletion of protein phosphatase 4 in human cells reveals essential roles in centrosome maturation, cell migration and the regulation of Rho GTPases. Int J Biochem Cell Biol 2008; 40:2315-32; PMID:18487071; http://dx.doi.org/10.1016/j.biocel.2008.03.021
13. Maroto B, Ye MB, von Lohneysen K, Schnelzer A, Knaus UG. P21-activated kinase is required for mitotic progression and regulates Plk1. Oncogene 2008; 27:4900-8; PMID:18427546; http://dx.doi.org/10.1038/onc.2008.131
14. Rai R, Phadnis A, Haralkar S, Badwe RA, Dai H, Li K, Lin SY. Differential regulation of centrosome integrity by DNA damage response proteins. Cell Cycle 2008; 7:2225-33; PMID:18635967; http://dx.doi.org/10.4161/cc.7.14.6303
15. Jin S, Gao H, Mazzacurati L, Wang Y, Fan W, Chen Q, Yu W, Wang M, Zhu X, Zhang C, et al. BRCA1 interaction of centrosomal protein Nlp is required for successful mitotic progression. J Biol Chem 2009; 284:22970-7; PMID:19509300; http://dx.doi.org/10.1074/jbc.M109.009134
16. Fabunmi RP, Wigley WC, Thomas PJ, DeMartino GN. Activity and regulation of the centrosome-associated proteasome. J Biol Chem 2000; 275:409-13; PMID:10617632; http://dx.doi.org/10.1074/jbc.275.1.409

17. Wigley WC, Fabunmi RP, Lee MG, Marino CR, Muallem S, DeMartino GN, Thomas PJ. Dynamic association of proteasomal machinery with the centrosome. J Cell Biol 1999; 145:481-90; PMID:10225950; http://dx.doi.org/10.1083/jcb.145.3.481
18. Didier C, Merdes A, Gairin JE, Jabrane-Ferrat N. Inhibition of proteasome activity impairs centrosome-dependent microtubule nucleation and organization. Mol Biol Cell 2008; 19:1220-9; PMID:18094058; http://dx.doi.org/10.1091/mbc.E06-12-1140
19. Gorbea C, Pratt G, Ustrell V, Bell R, Sahasrabudhe S, Hughes RE, Rechsteiner M. A protein interaction network for Ecm29 links the 26 S proteasome to molecular motors and endosomal components. J Biol Chem 2010; 285:31616-33; PMID:20682791; http://dx.doi.org/10.1074/jbc.M110.154120
20. Park S, Kim W, Tian G, Gygi SP, Finley D. Structural defects in the regulatory particle-core particle interface of the proteasome induce a novel proteasome stress response. J Biol Chem 2011; 286:36652-66; PMID:21878652; http://dx.doi.org/10.1074/jbc.M111.285924
21. Lee SY, De la Mota-Peynado A, Roelofs J. Loss of Rpt5 protein interactions with the core particle and Nas2 protein causes the formation of faulty proteasomes that are inhibited by Ecm29 protein. J Biol Chem 2011; 286:36641-51; PMID:21878651; http://dx.doi.org/10.1074/jbc.M111.280875
22. Ouyang H, Ali YO, Ravichandran M, Dong A, Qiu W, MacKenzie F, Dhe-Paganon S, Arrowsmith CH, Zhai RG. Protein aggregates are recruited to aggresome by histone deacetylase 6 via unanchored ubiquitin C termini. J Biol Chem 2012; 287:2317-27; PMID:22069321; http://dx.doi.org/10.1074/jbc.M111.273730
23. Xu P, Duong DM, Seyfried NT, Cheng D, Xie Y, Robert J, Rush J, Hochstrasser M, Finley D, Peng J. Quantitative proteomics reveals the function of unconventional ubiquitin chains in proteasomal degradation. Cell 2009; 137:133-45; PMID:19345192; http://dx.doi.org/10.1016/j.cell.2009.01.041
24. Wang H, Matsuzawa A, Brown SA, Zhou J, Guy CS, Tseng PH, Forbes K, Nicholson TP, Sheppard PW, Häcker H, et al. Analysis of nondegradative protein ubiquitylation with a monoclonal antibody specific for lysine-63-linked polyubiquitin. Proc Natl Acad Sci U S A 2008; 105:20197-202; PMID:19091944; http://dx.doi.org/10.1073/pnas.0810461105
25. Wen R, Li J, Xu X, Cui Z, Xiao W. Zebrafish Mms2 promotes K63-linked polyubiquitination and is involved in p53-mediated DNA-damage response. DNA Repair (Amst) 2012; 11:157-66; PMID:22055568; http://dx.doi.org/10.1016/j.dnarep.2011.10.015
26. Gack MU, Kirchhofer A, Shin YC, Inn KS, Liang C, Cui S, Myong S, Ha T, Hopfner KP, Jung JU. Roles of RIG-I N-terminal tandem CARD and splice variant in TRIM25-mediated antiviral signal transduction. Proc Natl Acad Sci U S A 2008; 105:16743-8; PMID:18948594; http://dx.doi.org/10.1073/pnas.0804947105
27. Kfoury Y, Nasr R, Favre-Bonvin A, El-Sabban M, Renault N, Giron ML, Setterblad N, Hajj HE, Chiari E, Mikati AG, et al. Ubiquitylated Tax targets and binds the IKK signalosome at the centrosome. Oncogene 2008; 27:1665-76; PMID:17891179; http://dx.doi.org/10.1038/sj.onc.1210804
28. Andersen JS, Wilkinson CJ, Mayor T, Mortensen P, Nigg EA, Mann M. Proteomic characterization of the human centrosome by protein correlation profiling. Nature 2003; 426:570-4; PMID:14654843; http://dx.doi.org/10.1038/nature02166
29. Müller H, Schmidt D, Dreher F, Herwig R, Ploubidou A, Lange BM. Gene ontology analysis of the centrosome proteomes of Drosophila and human. Commun Integr Biol 2011; 4:308-11; PMID:21980565; http://dx.doi.org/10.4161/cib.4.3.14806
30. Kawaguchi Y, Kovacs JJ, McLaurin A, Vance JM, Ito A, Yao TP. The deacetylase HDAC6 regulates aggresome formation and cell viability in response to misfolded protein stress. Cell 2003; 115:727-38; PMID:14675537; http://dx.doi.org/10.1016/S0092-8674(03)00939-5
31. Noguchi M, Yu D, Hirayama R, Ninomiya Y, Sekine E, Kubota N, Ando K, Okayasu R. Inhibition of homologous recombination repair in irradiated tumor cells pretreated with Hsp90 inhibitor 17-allylamino-17-demethoxygeldanamycin. Biochem Biophys Res Commun 2006; 351:658-63; PMID:17083915; http://dx.doi.org/10.1016/j.bbrc.2006.10.094
32. Quanz M, Herbette A, Sayarath M, de Koning L, Dubois T, Sun JS, Dutreix M. Heat shock protein 90α (Hsp90α) is phosphorylated in response to DNA damage and accumulates in repair foci. J Biol Chem 2012; 287:8803-15; PMID:22270370; http://dx.doi.org/10.1074/jbc.M111.320887
33. Davies AE, Kaplan KB. Hsp90-Sgt1 and Skp1 target human Mis12 complexes to ensure efficient formation of kinetochore-microtubule binding sites. J Cell Biol 2010; 189:261-74; PMID:20404110; http://dx.doi.org/10.1083/jcb.200910036
34. de Cárcer G. Heat shock protein 90 regulates the metaphase-anaphase transition in a polo-like kinase-dependent manner. Cancer Res 2004; 64:5106-12; PMID:15289312; http://dx.doi.org/10.1158/0008-5472.CAN-03-2214
35. de Cárcer G, do Carmo Avides M, Lallena MJ, Glover DM, González C. Requirement of Hsp90 for centrosomal function reflects its regulation of Polo kinase stability. EMBO J 2001; 20:2878-84; PMID:11387220; http://dx.doi.org/10.1093/emboj/20.11.2878
36. Peng HM, Morishima Y, Clapp KM, Lau M, Pratt WB, Osawa Y. Dynamic cycling with Hsp90 stabilizes neuronal nitric oxide synthase through calmodulin-dependent inhibition of ubiquitination. Biochemistry 2009; 48:8483-90; PMID:19642705; http://dx.doi.org/10.1021/bi901058g
37. Kundrat L, Regan L. Identification of residues on Hsp70 and Hsp90 ubiquitinated by the cochaperone CHIP. J Mol Biol 2010; 395:587-94; PMID:19913553; http://dx.doi.org/10.1016/j.jmb.2009.11.017
38. Johnston JA, Ward CL, Kopito RR. Aggresomes: a cellular response to misfolded proteins. J Cell Biol 1998; 143:1883-98; PMID:9864362; http://dx.doi.org/10.1083/jcb.143.7.1883
39. Moudjou M, Bornens M. Cell biology: a laboratory handbook, ed. J.E. Celis. San Diego: Academic Press; 1994. Isolation of centrosomes from cultured animal cells; p. 595–604.

Wada et al. Journal of Clinical Bioinformatics 2014, 4:3
http://www.jclinbioinformatics.com/content/4/1/3

JCBi JOURNAL OF CLINICAL BIOINFORMATICS

RESEARCH Open Access

Development of detection method for novel fusion gene using GeneChip exon array

Yusaku Wada[1,4*], Masaaki Matsuura[1,2], Minoru Sugawara[1], Masaru Ushijima[1,2], Satoshi Miyata[3], Koichi Nagasaki[1], Tetsuo Noda[1,2] and Yoshio Miki[1,2]

Abstract

Background: Fusion genes have been recognized to play key roles in oncogenesis. Though, many techniques have been developed for genome-wide analysis of fusion genes, a more efficient method is desired.

Results: We introduced a new method of detecting the novel fusion gene by using GeneChip Exon Array that enables exon expression analysis on a whole-genome scale and TAIL-PCR. To screen genes with abnormal exon expression profiles, we developed computational program, and confirmed that the program was able to search the fusion partner gene using Exon Array data of T-cell acute lymphocytic leukemia (T-ALL) cell lines. It was reported that the T-ALL cell lines, ALL-SIL, BE13 and LOUCY, harbored the fusion gene NUP214-ABL1, NUP214-ABL1 and SET-NUP214, respectively. The program extracted the candidate genes with abnormal exon expression profiles: 1 gene in ALL-SIL, 1 gene in BE13, and 2 genes in LOUCY. The known fusion partner gene NUP214 was included in the genes in ALL-SIL and LOUCY. Thus, we applied the proposed program to the detection of fusion partner genes in other tumors. To discover novel fusion genes, we examined 24 breast cancer cell lines and 20 pancreatic cancer cell lines by using the program. As a result, 20 and 23 candidate genes were obtained for the breast and pancreatic cancer cell lines respectively, and seven genes were selected as the final candidate gene based on information of the EST data base, comparison with normal cell samples and visual inspection of Exon expression profile. Finding of fusion partners for the final candidate genes was tried by TAIL-PCR, and three novel fusion genes were identified.

Conclusions: The usefulness of our detection method was confirmed. Using this method for more samples, it is thought that fusion genes can be identified.

Keywords: Exon array, Fusion gene, Chromosome rearrangement

Background

It is well known that cancer is caused by gene abnormalities. There are many types of abnormalities in the genome of cancer cells, including gene fusion because of chromosome rearrangement. The discovery of a characteristic small chromosome, called Philadelphia chromosome, in chronic myeloid leukemia, is the first recurrent chromosome rearrangement to be seen in a human cancer [1]. This rearrangement was eventually identified as a translocation between chromosome 9 and 22 [2], resulting in the fusion of the *BCR* gene on chromosome 22 with the *ABL1* gene on chromosome 9, *BCR-ABL1* [3]. Because many chromosomal abnormalities and fusion genes have been discovered by the development of experimental techniques, it has been shown that such fusion genes and chromosomal abnormalities are causes of cancer. Thus, the importance of chromosomal abnormalities and fusion genes in cancer has been recognized.

It is also known that fusion genes have a key role in oncogenesis in hematological tumors and sarcomas. Since fusion genes are closely related to the clinical and pathological features of tumors, they provide important clues for diagnosis. In addition, fusion genes are regarded as attractive targets of molecular targeted treatments because of their high specificity to tumors.

So far, fusion genes have been found less frequently in common solid cancers, but some reports on prostate [4] and lung carcinomas [5] show that fusion genes contribute

* Correspondence: ywada@fasmac.co.jp
[1]Genome Center, Japanese Foundation for Cancer Research, 3-8-31 Ariake, Koto-ku, Tokyo 135-8550, Japan
[4]Current address: FASMAC Co., Ltd, 3088 Okata, Atsugi City, Kanagawa 243-0041, Japan
Full list of author information is available at the end of the article

significantly to the development of these malignancies. It is predicted that fusion genes have important roles in many other kinds of epithelial tumors [6]. In late years, various fusion genes came to be discovered by many kinds of cancers [7].

Although many technologies are used for the genome-wide screening of fusion genes, there are not yet any versatile methods. Karyotyping requires the availability of fresh, vital cells for short-term culturing to obtain metaphase chromosomes, and it has low resolution. Array comparative genomic hybridization (array CGH) cannot detect fusion genes without genomic copy number change [8]. Recent developments of high-throughput sequencing technologies provide a powerful tool [9-12]. But these technologies are as yet limited by the number of samples that can be analyzed at acceptable cost.

Affymetrix GeneChip Human Exon 1.0 ST Array (Exon Array) is a whole-genome exon expression analysis tool. About 5.5 million probes are being designed on the array, and they compose about 1.4 million probe sets (in principle, the probe set is composed of four probes, and one expression intensity is calculated from one probe set). The expression of almost all exons can be analyzed using the Exon Array, and it enables genome-wide alternative splicing analysis. Each probe set has an ID, and belongs to a transcript cluster that corresponds to a gene. Annotations are given to the probe sets, and are available to the public at Affymetrix NetAffx (http://www.affymetrix.com/analysis/index.affx). The probe sets are classified into three evidence levels according to the quality of evidence supporting the transcription of the target genomic sequence. The three evidence levels are presented in decreasing order of confidence: "core" (RefSeq and full-length mRNAs), "extended" (ESTs, syntenic rat and mouse mRNAs) and "full" (ab-initio computational predictions). Simultaneously, the probe sets are annotated with hybridization targets that describe cross-hybridization potential. The hybridization targets are shown in decreasing order of uniqueness: "unique", "mixed", and "similar".

In this report, a method to detect abnormal gene structures, including gene fusion, was developed using Exon Array. Using this methodology and TAIL-PCR, novel fusion genes were discovered in breast and pancreatic cancer cell lines. Breast cancer is a heterogeneous disease encompassing a wide variety of pathological features and a range of clinical behavior [13]. These are underpinned at the molecular level by complex components of genetic alterations that affect cellular processes [14]. Therefore, it is possible to contribute for understanding of the heterogeneity and diagnosis with high accuracy by discovering novel fusion genes. Pancreatic cancer is a highly aggressive tumor with no proven curative chemotherapy or radiation therapy, having extremely poor prognosis [15]. The discovery of a fusion gene in pancreatic cancer can lead to molecular target therapy, with the possibility of offering an effective treatment method for pancreatic cancer.

Methods

Samples

Twenty-four breast cancer cell lines (AU565, BT474, DU4475, HCC38, HCC70, HCC202, HCC1143, HCC1187, HCC1419, HCC1428, HCC1569, HCC1806, HCC1954, MCF7, MDA-MB-157, MDA-MB-231, MDA-MB-330, MDA-MB-361, MDA-MB-435S, MDAMB-468, SK-BR-3, UACC812, UACC893, ZR-75-1) were obtained from American Type Culture Collection (ATCC), and maintained in under the conditions recommended by the supplier. Twenty pancreatic cancer cell lines (MA005, MA006, PA018, PA022, PA028, PA043, PA051, PA055, PA086, PA090, PA103, PA107, PA109, PA167, PA173, PA182, PA195, PA199, PA202, PA215) were established at Genome Center, Japanese Foundation for Cancer Research (JFCR). Two vials of normal mammary epithelial cells (HMEC), which were donated from different subjects, were obtained from Takara Bio Inc. A non-tumorigenic human breast epithelial cell line (MCF10A) was obtained from ATCC. These were maintained using TaKaRa MEGM BulletKit (Takara Bio Inc, Otsu, Japan) according to the manufacturer's instructions. A clear cell sarcoma cell line "SarcomaA" was provided by Dr. Nakamura at Cancer Institute, JFCR.

Samples of tumor tissues were obtained from a series of patients with breast or pancreatic cancer who underwent surgery at the JFCR Hospital. All samples were snap-frozen in liquid nitrogen within 1 h after surgery and stored at −80°C. Before RNA was prepared, laser-captured microdissection (LCM) using a Leica Microsystems AS LMD 600 (Leica Microsystems, Wetzlar, Germany) was performed to ensure that only tumor cells were dissected. LCM was conducted in all tumor samples.

Open access exon array data

Exon Array CEL files of 17 T-cell acute lymphocytic leukemia (T-ALL) cell lines (ALL-SIL, BE13, CEM, DND41, DU528, JURKAT, KOPTK1, LOUCY, MOLT13, MOLT16, MOLT4, PF382, RPMI8402, SUPT11, SUPT13, SUPT7, TALL1) were obtained from NCBI Gene Expression Omnibus database (Series GSE9342, http://www.ncbi.nlm.nih.gov/geo/query/acc.cgi?acc=GSE9342). It was reported that ALL-SIL, BE13 and LOUCY harbored fusion genes NUP214-ABL1, NUP214-ABL1, and SET-NUP214, respectively [16,17].

Total RNA extraction and cDNA synthesis

Total RNA was extracted from the cells or the tissues by RNeasy Mini Kit according to the manufacturer's instructions (Qiagen, Valencia, CA). 1 μg of total RNA was reverse transcribed to synthesize template cDNA by a

random primer using the Invitrogen SuperScriptIII First-Strand Synthesis System(Life Technologies, Carlsbad, California), and 20 μl synthesized cDNA was diluted 500 times with Tris/HCl buffer.

Exon array experiment

Exon Array data was generated according to the manufacturer's instructions. Ribosomal RNA was removed from 1 μg of total RNA using Invitrogen RiboMinu Transcriptome Isolation Kit, and amplified cDNA was synthesized using GeneChip WT cDNA Synthesis and Amplification Kit. To make hybridization probes, amplified cDNA was fragmented and biotin-labeled using GeneChip WT Terminal Labeling Kit. The hybridization probes were hybridized to GeneChip Human Exon 1.0 ST Array at 45°C in a hybridization oven at 60 rpm for 16 h, and washed in Fluidics Station 450 using GeneChip Hybridization Wash, and Stain Kit. The array was scanned on GeneChip Scanner 3000 7G. To implement signal summarization, expression intensities for the "core" ProbeSet were calculated using linear normalization and the average-difference method from Affymetrix Power Tools. The median intensity of all arrays was adjusted linearly to 100.

Fusion gene screening program

The program was developed to detect fusion genes with an exon expression profile similar to that of *EWSR1* and *ATF1* in a clear cell sarcoma cell line, SarcomaA. Details of the program are shown in 1–8

1. To exclude the influence of non-specific hybridization, only probe sets with Hybridization Target "unique" were used.
2. To exclude probe sets that showed extremely low signal intensities in all samples, only probe sets with 30 or higher signal intensity in at least one sample were used.
3. To use probe sets corresponding to known exon sequence, only probe sets with Evidence Level "Core" were used.
4. To avoid the influence of alternative splicing and non-specific hybridization, 5–8 were performed for probe sets of the Transcript Cluster with 8 or more probe sets for which conditions 1–3 were met.
5. To compare expression levels among probe sets in each sample, the rank of each probe set of the sample was decided based on the signal intensity.
6. One transcript cluster with probe sets for which conditions 1–3 were met were separated into 5′ and 3′ terminal groups at all possible cut off points so that each terminal group contains 4 or more probe set. ("cut off point" is only used in our algorithm to divide genome region into 5′ or 3′ terminal groups) For each sample, the average rank of probe sets in 5′ and 3′ terminal groups were calculated, respectively.
7. To detect genes with a clear expression level change before and behind the cut off points, it is confirmed that the difference in the average ranks of 5′ and 3′ terminal groups was 70% or more of the number of samples.
8. To reduce the possibility of false positives by measurement errors, the cut off points were identified as breakpoints only when at least one of the standard deviations of probe set ranks in 5′ or 3′ terminal groups was 2.0 or lower. Transcript clusters with candidate breakpoints were identified as candidate genes.

Our program for detecting fusion genes was written in Fortran95. One more program for drawing exon expression pattern of samples and location of exon in the genome database, as shown in the figures in this paper, was written in statistical language of R. We used Windows PC for both programs as a platform. Any machines installed with the Fortran95 and R would be able to be used for our purpose. Our source program will be available on direct request to the corresponding author.

Evaluation of candidate genes

To take transcript isoforms of candidate genes into consideration, the transcript isoform information registered in UCSC Genome Browser (http://genome.ucsc.edu/cgi-bin/hgGateway) "UCSC Gene" and "Ensembl Gene Prediction" was used. When the exon/intron structure of the aberrant transcript predicted from the exon expression profile of the candidate gene was similar to the registered transcript isoform, the gene was excluded from candidate genes. When the candidate gene (Transcript Cluster) corresponds to two or more RefSeq genes in UCSC Genome Browser, the gene was also excluded from candidate genes. When the exon expression profile of the screened sample in candidate genes was similar to the profile of the reference sample, the gene was excluded from candidate genes. Moreover, exon expression profiles of the candidate genes were evaluated by visual inspection in detail.

TAIL-PCR, RT-PCR and one step RT-PCR

TAIL-PCR (thermal asymmetric interlaced-PCR) was performed with a slight modification of the original Yao-Guang Liu and Yuanling Chen's high-efficiency TAIL-PCR protocol [18] for the identification of fusion counterpart. The primers and thermal cycling condition are shown in Tables 1, 2, and 3. For RT-PCR, TaKaRa Ex Taq Hot Start Version and 2 μl synthesized cDNA as template were used. Thermal cycling was carried out under the following conditions: 1 min at 95°C followed by 35 cycles of